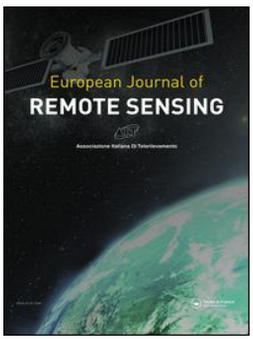

European Journal of Remote Sensing

ISSN: (Print) 2279-7254 (Online) Journal homepage: http://www.tandfonline.com/loi/tejr20

Simplified radiometric calibration for UAS-mounted multispectral sensor

Faheem Iqbal, Arko Lucieer & Karen Barry

To cite this article: Faheem Iqbal, Arko Lucieer & Karen Barry (2018) Simplified radiometric calibration for UAS-mounted multispectral sensor, European Journal of Remote Sensing, 51:1, 301-313, DOI: 10.1080/22797254.2018.1432293

To link to this article: https://doi.org/10.1080/22797254.2018.1432293

Published online: 06 Feb 2018.

EUROPEAN JOURNAL OF REMOTE SENSING, 2018
VOL. 51, NO. 1, 301–313
https://doi.org/10.1080/22797254.2018.1432293

Taylor & Francis
Taylor & Francis Group

Simplified radiometric calibration for UAS-mounted multispectral sensor

Faheem Iqbal [a], Arko Lucieer[b] and Karen Barry[b]

[a]School of Land and Food, University of Tasmania, Hobart, Australia; [b]School of Technology, Environments and Design, College of Sciences and Engineering, University of Tasmania, Australia

ABSTRACT

Unmanned aircraft system (UAS) in combination with multispectral sensors stimulate the utilisation of site-specific technologies to manage crop production according to intrafield variability. Crop monitoring requires accurate calibration. However, radiometric calibration methods in practice are difficult to implement for UAS remote sensing as every single image requires correction due to smaller field of view and changes in light. Therefore, this paper proposes an easy radiometric calibration process for UAS-based miniature multiple camera array multispectral sensor. Results showed linear relationship between spectral reflectance and raw DN values with *y*-intercept value compatible with zero. It is the minimal possible surface reflectance recorded by sensor and can be used as a first point for equation development. The spectral quantification of white pseudo target was used as a second point of equation. Quantitative spectral information was generated by developing equation for every single image. An accuracy assessment was undertaken by comparing image-driven reflectance values against reflectance values measured in the field from soil and crop. The overall accuracy based on the root mean square error for the six bands ranged from 0.025% to 0.064%. The results of this study showed that the proposed method can be used for the calibration of UAS-based multispectral image .

ARTICLE HISTORY
Received 8 June 2017
Revised 3 January 2018
Accepted 21 January 2018

KEYWORDS
Radiometric calibration; empirical line; UAS; remote sensing

Introduction

Precision agriculture generally involves better management of farm inputs at the right place and the right time to optimise crop yield (Mulla, 2013). While the general practice in field management is to apply even applications of irrigation, pesticides and fertilisers etc. throughout the paddock. Remote sensing (RS) technology has paved a great importance in the field of sustainable agriculture (Zhang & Kovacs, 2012). The use of RS technologies provides data to retrieve crop variability information (Carbone, Narumalani, & King, 1996; French, Hunsaker, & Thorp, 2015; Morel et al., 2014; Oudemans, Pozdnyakova, Hughes, & Rahman, 2002; Stadler et al., 2015; Zarco-Tejada, Ustin, & Whiting, 2005a; Zhang & Kovacs, 2012). RS helps in the division of a field into different variability zones that facilitates crop management by customising variable inputs (Larson & Robert, 1991; Zhang, Wang, & Wang, 2002). On the global scale, studies have used satellite RS to monitor plant growth by computing different spectral indices (Baluja et al., 2012; Berni, Zarco-Tejada, Sepulcre-Canto, Fereres, & Villalobos, 2009; Brandao, Sofiatti, Bezerra, Ferreira, & Medeiros, 2015; Kaur, Singh, Singh, & Thind, 2015; Saari et al., 2011; Stagakis, González-Dugo, Cid, Guillén-Climent, & Zarco-Tejada, 2012; Waine, Simms, Taylor, & Juniper, 2014; Zarco-Tejada et al., 2013). Crop health information derived from satellite data have a potential to forecast economic return and help policy makers to take precautionary measures for food security at national level (Bastiaanssen & Ali, 2003; Bastiaanssen, Molden, & Makin, 2000; Fedotov & Osmani, 2010; Morel et al., 2014; Series & Statistics,). However, in majority part of the world agriculture is mainly driven by small farms (Thornton, 2002). Land owners of small farms need to grow multiple crops in order to fulfil their food requirements, resulting in enormous variability of crop type and management practices within the farm. Usually, this variability cannot be captured over the canvas of satellite imagery due to the small size of the farm and low spatial resolution of imageries (Boschetti, Flasse, & Brivio, 2004; Leroux, Jolivot, Bégué, Lo, & Zoungrana, 2014). This variability restricts the use of satellite imagery at local scale due to spatial resolution (Lausch et al., 2013). Moreover, crop management on farm scale requires availability of crop information at specific time during the crop cycle and requires repeated measurements (Cheng, Zarco-Tejada, Riano, Rueda, & Ustin, 2006; Cohen, Alchanatis, Meron, Saranga, & Tsipris, 2005; Iqbal, 2011; Zarco-Tejada, Miller, Morales, Berjon, & Aguera, 2004). Thus, satellite RS is not a suitable option for small land farmers (Stafford, 2000). There exist alternatives such as piloted airborne platforms that allow to acquire very high spatial resolution data at a required time, but are difficult to

CONTACT Faheem Iqbal faheem.engr@gmail.com School of Land and Food, University of Tasmania, Hobart, Australia

use due to their high costs (Rango et al., 2009). Recently, growing attention has been given to the use of unmanned aircraft systems (UASs) to overcome the limitations of satellite RS, especially where small farm areas have to be monitored (Harwin & Lucieer, 2012; Lucieer, De Jong, & Turner, 2013; Lucieer, Malenovský, Veness, & Wallace, 2014; Swain, Thomson, & Jayasuriya, 2010; Torres-Sánchez, López-Granados, & Peña, 2015; Zhu, Wang, Deng, & Harmon, 2010; Zhu et al., 2010). The use of UAS as a RS platform has demonstrated the potential for small farm management by providing multi-temporal data (Bendig, Bolten, & Bareth, 2013; Zhou et al., 2017). It provides flexibility in acquisition at much lower costs as compared to aerial and satellite data. Images captured using UAS generally have spatial resolution within a few centimetres. Therefore, UAS acquired images could be a practical alternative to aerial and satellite RS. For small farm management, UAS RS-driven spectral signatures have been used to estimate biophysical characteristics of plants (Baluja et al., 2012; Berni, Zarco-Tejada, Suarez, & Fereres, 2009b; Jaakkola et al., 2010; Mäkynen, Saari, Holmlund, Mannila, & Antila, 2012; Zhang & Kovacs, 2012) to monitor plant growth and health (Bendig et al., 2014; Berni, Zarco-Tejada, Suarez, & Fereres, 2009a; Kelcey & Lucieer, 2012; Saari et al., 2011; Zhu et al., 2010).

UAS-based RS technology has developed remarkably and customised sensors are available for agricultural applications (Zhang & Kovacs, 2012). Continuous development in the field of electronics allows the production of lightweight navigation systems and controllers which makes UASs cost effective (Joseph, Aerts, Vandenbossche, Thielens, & Martens, 2016). On the other hand, the latest developments in plastic technology are replacing metals (Ajayan & Tour, 2007; Zhu, Lowe, & Langdon, 2004) and high-performance polymer materials providing same mechanical strength with dramatic reduction in weight, which allows carrying of more payload and results in increase in UAS flight time (Ajayan & Tour, 2007). For these reasons, the use of UAS RS for small agriculture farms is increasing and its use is anticipated to increase in future (Baluja et al., 2012; Stellman, Olchowski, & Michalowicz, 2001; Uto, Seki, Saito, & Kosugi, 2013; Zhang & Kovacs, 2012).

UASs are often operated under suboptimal conditions, such as below a full or partial cloudy cover. Despite the challenging conditions, the images must be processed accurately so that object characteristics can be interpreted on a quantitative geometric and radiometric basis using the data. Radiometric calibration of images is a prerequisite, especially for precision agriculture (Moran et al., 2001), where change in spectral signatures across the paddock is used to develop management zones (Bakhsh and Kanwar 2006; Pinter et al., 2003; Whiting et al., 2006). The data retrieved from an image are in the form of digital numbers (DNs), which is not a true representative of the surface reflectance (Del Pozo, Rodríguez-Gonzálvez, Hernández-López, & Felipe-García, 2014). The sensor records the radiance and converts it to DNs, which is not a quantitative value (Smith & Milton, 1999) and changes with illumination conditions and consistency of sensor.

UAS campaigns with smaller field of view (FOV) result in large number of very high resolution images over a small paddock (Del Pozo et al., 2014; Oøvergaard, Isaksson, Kvaalc, & Korsaeth, 2010; Wang & Myint, 2015). Smaller FOV results in variation in range of DN values and generates an un-reliable data (Herrero-Huerta, Hernández-López, Rodriguez-Gonzalvez, González-Aguilera, & González-Piqueras, 2014; Warren et al., 2011), which can be associated to change in illumination (Wang & Myint, 2015). Therefore, for reliable crop zonation each UAS-based image needs to be radiometrically corrected to maintain the spectral consistency throughout the campaign (Smith & Milton, 1999).

Several levels of radiometric correction for RS data are available (Chavez, 1989; Smith & Milton, 1999; Vicente-Serrano, Pérez-Cabello, & Lasanta, 2008). The first level is to convert the sensor DNs to sensor radiance, which requires camera calibration information. The second step is transformation of the sensor radiance to radiance at the earth surface (Mattar et al., 2014), which requires removal of atmospheric distortions. Multiple methods have been developed to remove the effect of atmospheric distortion including radiative transfer model and empirical line method (Miura & Huete, 2009; Moran et al., 2001; Saari et al., 2011; Smith & Milton, 1999; Wang & Myint, 2015).

The altitude of UAS campaigns is restricted by Civil Aviation Safety Authority (CASA) Australia for remote pilot aircraft and allows flight below 120 m. In case of small farms, UAS is flown around 50–100 m that passes through a very small atmospheric column. Therefore, the difference of radiance at sensor and surface is minimal, and is thus, ignored. The use of empirical line correction method is based on relationship between DN value and surface reflectance in which the DN values are converted to the units of reflectance (Moran et al., 2001; Smith & Milton, 1999; Wang & Myint, 2015). The role of ground targets in radiometric correction of imagery is vital and thus, reflactance data of targets are used for the calibration and validation of data (Baugh & Groeneveld, 2008; Staben, Pfitzner, Bartolo, & Lucieer, 2012). On field, the reflectance of ground targets is recorded with spectrometer and the DN values of the same targets are extracted from the image. The radiance values from the image are plotted on the independent axis and the reflectance values from the ground targets are plotted on

dependent axis. This gives a linear or near-linear relationship, depending on the number of targets used (Karpouzli & Malthus, 2003; Smith & Milton, 1999; Stow, Hope, Nguyen, Phinn, & Benkelman, 1996).

Most researchers have used two calibration targets (black and white) to cover the range of dark and bright pixels in the image (Baugh & Groeneveld, 2008; Chavez, 1989; Del Pozo et al., 2014; Herrero-Huerta et al., 2014). This process assumes that the distribution of DN to reflectance within image is linear (Baugh & Groeneveld, 2008; Smith & Milton, 1999). However, this is not always true, especially when working with crops (Stow et al., 1996). Some researchers use multiple calibration targets to improve the calibration accuracy and assume that illumination is uniform throughout the campaign with lambertian properties and the relationship remains the same for all images (Staben et al., 2012). However, in case of multiple images with smaller FOV, this case is not always true due to illumination conditions and therefore, every image needs to be calibrated to achieve consistency in results (Stow et al., 1996; Wang & Myint, 2015). Dozens of calibrations targets are required over a field such that each UAV-based acquired image should capture one target for the purpose of calibration. As the calibration targets with lambertian properties are very expensive making the overall field campaign cost intensive, thus, a feasible, accurate and cost effective method needs to be developed for the radiometric correction of UAS images. Therefore, for this study, photo targets were tested as pseudo calibration targets in order to make the campaign more cost effective. The objective of this study was to test the performance of pseudo photo targets in place of calibration targets by developing a relationship between multiple image derived DN values acquired through miniature multiple camera array (Mini-MCA) sensor and field measured reflectance. The relationship developed by using pseudo photo targets was then utilised to convert image DN values to surface reflectance for achieving radiometric calibration of UAV-based imageries.

Materials and methods

Materials

This research was conducted at a research farm of University of Tasmania (42°47′50.84″S, 147°25′33.06″E, attitude 32 m), at Cambridge located around 20 km east of Hobart, Tasmania, Australia (Figure 1). In summer 2014, a commercial crop was sown at a selected paddock. UAS campaigns were conducted along two transects almost perpendicular to each other. The images acquired from flight campaign conducted over transect one was used for calibration equation development and imagery acquired from transect two was used to check the consistency and calibration coefficient extraction.

In this study, Mini-MCA was used (Figure 2), which is a low-cost influential instrument used for crop mapping. It can provide the data to investigate the development stages of the crop. This sensor was mounted on multirotor aircraft to acquire the spectral images from multiple discrete bands. For the field spectral data, ASD FieldSpec 3 spectroradiometer (Analytical Spectral Device, Inc., Boulder, co, USA) was used to collect the spectral reflectance of photo targets and calibration targets. Details of all the steps undertaken are elaborated in subsequent sections.

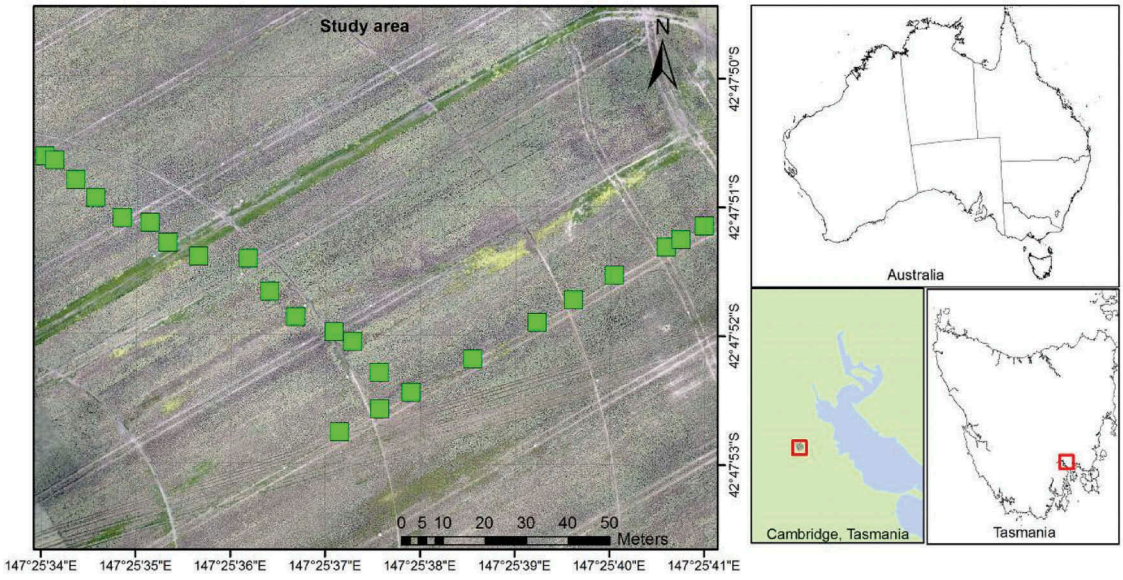

Figure 1. The general location of study site and the overview of the image obtained from UAS showing sampling locations in green for surface reflectance comparison. Full color availabel online

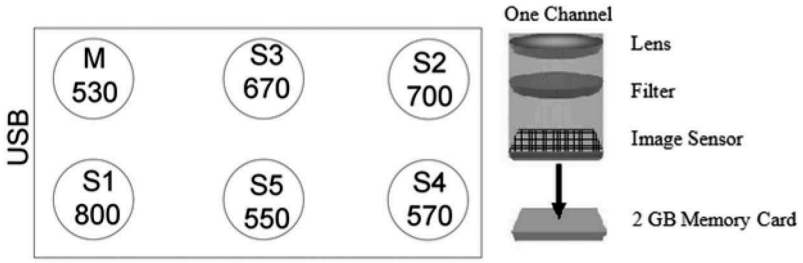

Figure 2. Modified tetracam miniature multiple camera array (Mini-MCA).

Multispectral sensor

A multispectral sensor is a powerful and dominating instrument for environmental RS (Stow et al., 1996). It can provide the data to investigate the development of the crop (Del Pozo et al., 2014). UAV-mounted multispectral sensors can acquire the spectral data from multiple discrete bands, which can be used for the computation of indices (Herrero-Huerta et al., 2014). Studies have been published in past to highlight the potential use of indices in crop yield modelling (Dempewolf et al., 2014; Geipel, Link, & Claupein, 2014; Kross, McNairn, Lapen, Sunohara, & Champagne, 2015; Papadavid, Hadjimitsis, Toulios, & Michaelides, 2011; Zarco-Tejada, Ustin, & Whiting, 2005b). The Mini-MCA of Tetracam Inc. was used for this research. It consists of an array of six individual channels, each channel consisting of a lens, a filter, a memory card and a complementary metal-oxide-semiconductor (CMOS) sensor that records the light passing through the filter within a channel as an image on the memory card. The spectral response of image sensors is uniform through the range with optimum sensitivity (100%) between 750 and 800 nm and gradual decrease to 20% at 450 nm in visible region and 1050 nm in near-infrared region (Kelcey & Lucieer, 2012). Every channel of Mini-MCA has a place of band-pass spectroscopic filters and is placed between lens and image sensor. Spectroscopic filters restrict radiation allowing a narrow band of wavelength to reach the image sensor. The amount of light received by each image sensor is directly dependent on the band-pass filter. Camera sensors produce finest image at full width half maximum (FWHM) of 10 nm as it provides optimum light, although, exceptions prevail at the far ends of the sensors sensitivity range. In this case, more light passes through the far end filter and is balanced by the sensor's diminished affectability. In our study, we used the filters with a central wavelength of 530, 550, 570, 670, 700 and 800 nm. Corresponding FWHM and peak transmission wavelength of each filter are listed in Table 1. Filters are interchangeable depending upon the purpose of UAS campaign.

Table 1. Mini-MCA channel specifications.

Channel	Filter	FWHM	Peak wavelength (nm)	Band width range (nm)	Peak transmission (%)
Main	530	10	530.50	510–550	59.71
S1	800	10	799.60	780–820	59.61
S2	700	10	702.20	680–720	69.44
S3	670	10	670.50	650–690	70.17
S4	570	10	571.80	550–590	62.99
S5	550	10	549.60	530–550	55.01

Spectral campaign of calibration targets

To measure field reflectance, 5 radiometric calibration targets and 20 photo targets (pseudo targets) were used in this study. All five calibration targets were placed along the transect and spectral measurements of each calibration target were taken using ASD FieldSpec3 spectroradiometer (Analytical Spectral Device, Inc., Boulder, co, USA). ASD FieldSpec3 is a passive device which depends on solar illumination and acquires the data from 325 to 1075 nm. Reflectance measurements were taken during the flight campaign (1:00 pm to 2:00 pm) under solar light. During spectral data collection, spectroradiometer calibration measurements were taken with a reference panel (white colour Spectralon) and dark current before and after taking readings from radiometric calibration targets. A total of 20 spectral readings were taken from each target from a distance of 1 m without blocking sunlight with a sample count of 15. Every spectral reading per calibration panel was averaged for further analysis and average of all 20 spectral readings was used for image calibration analysis.

UAS campaign acquired hundreds of very high resolution images over a small farm and every image required one calibration target for calibration. It is not feasible to place a large number of radiometric calibration targets during each flight campaign as it increases the cost of each campaign. Moreover, this UAV sensor does not cater for the illumination-specific data and thus requires more detailed calibration data. As the intensity of ambient light varies, the amount of reflected light energy from the surface will alter resulting in inaccurate information. To cope with illumination variability, accurate calibration is imperative. Therefore, this study tested one pseudo calibration target per image, thus, distributing 20 pseudo targets throughout the study area of around 60 m× 180 m to make sure one target is captured by each image. For this purpose, matte finish plastic boards of 0.5 m× 0.5 m photo targets were used for

geometric correction as pseudo radiometric calibration targets for each image. Spectral readings from white portion of pseudo targets were measured using spectroradiometer. To make sure the readings were taken from the white portion of the targets, pointing light of the spectroradiometer was used as a marker and measurements were taken from a distance of 0.5 m. The calibration target was then tested for lambertian material properties for which, 20 spectral measurements were taken from 4 different viewing angles. To compare the collected field spectra with Mini-MCA imagery, spectral signals were resampled to Mini-MCA band positions. In this research, FWHM values and central wavelength of each Mini-MCA band values were used to resample the reference field measured spectral signatures. This was carried out using R package Prospectr, which uses Gaussian model with FWHM spacing (Stevens & Ramirez-Lopez, 2014).

UAS platform

In this study, UAV platform was used for the collection of multispectral sensor data with a Multirotor Oktokopter. The payload capacity of UAS platform used in this study was 2 kg. The flight duration was 5–10 min, depending on batteries and payload. To maintain near nadir position of sensor, gimbal was used. An on-board Autopilot system with GPS, 3D advanced compass and barometric altimeter permits the system to follow the predefined flight path. According to CASA laws, flying height within three nautical miles of aerodrome is restricted and UAV cannot be operated above 120 m. For this research, as the study site was within three nautical miles from controlled aerodrome, thus, it was necessary to maintain an allowed range of flying height during the campaign. Flying height being a crucial factor was calculated beforehand based on the size of calibration target. For the purpose of calibration, multiple number of pixels from each calibration target need to be present, for which, flight height was calculated using the relation between flight height and pixel size. Moreover, the length and pitch of propeller time and distance travelled by each flight were calculated to manage the number of batteries required to complete the mission. A planned campaign was conducted at the altitude of ~45 m to acquire a pixel resolution of 3 cm using four flights. UAS system was equipped with gimbal to mount the Mini-MCA camera. Finally, 500 images were captured from the study site.

Image processing

UAS campaign captured 500 images that required enormous rectification followed by radiometric calibration to obtain seamless, homogenous spectral reflectance data from a non-homogenous raw image. To reduce the processing load, 240 images were selected by eliminating every second image and systematic noise and vignetting affect were corrected (Kelcey & Lucieer, 2012). To completely remove the influence of vignetting, outer edges of each image were removed. As Mini-MCA consists of six separate channels and the channel images produced are not co-registered with each other, therefore, all channel images were geometrically registered before conversion of DN to surface reflectance (Turner, Lucieer, & Watson, 2012).

Radiometric calibration

All corrected images were converted to 10 bit tagged image file format. Multiple overlapping images capturing the calibration targets were selected for analysis. Points were generated on a centre point of each radiometric and pseudo calibration target and a boxed buffer was generated over each target. Vectors of overlapped boxes were converted to raster format with pixel size equal to image. Each pixel of overlapped layer was converted to points and each point was used to extract the DN values from multiple images. To compare *in situ* measurements with imagery, it was found that DN value of every pixel recorded by sensor had a direct relationship with surface reflectance of target. The relationship can be represented by the following simple linear equation.

$$\text{Surface } \textit{reflectence} = \textit{slope} \times \textit{DN} \pm \text{intercept}.$$

For ease of analysis, polygon grid was used for extracting image DN values from each calibration and pseudo target for all bands. This polygon grid was used to calculate the statistics of DN values from each target. Therefore, the resulting 40 pixel values of each target (calibration and pseudo) were used to compute the mean DNs of corresponding targets for each image separately. The DN values of multiple images were then plotted against the *in situ* mean convolved reflectance values at central wavelength of each sensor image. Relationships were computed between the sensor corrected spectral bands generated by the mini-MCA and the corresponding at-surface reflectance measurements. The linear relationship between the DN and reflectance showed y-intercept comparable to zero. Theoretically, it is the minimum reflectance value which can be recorded by an image sensor and is an intrinsic property of sensor that cannot change abruptly. Multiple equations were developed from overlapping images to check the consistency of minimum possible reflectance recoded by sensor. Moreover, the relationship between calibration targets and pseudo targets was tested by computing multiple equations. Finally, zero reflectance being minimum possible reflectance recorded by the sensor was used as one data point and maximum reflectance point was used as pseudo target point. Predication equation for each image was

developed using resampled spectral and DN values of pseudo target. Sensor measurements were converted into reflectance measurements by applying each linear equation to its corresponding image.

Ground comparison and verification

The overall accuracy of the proposed method was assessed by comparing image-driven reflectance values with the field measured reflectance values. Summary statistics were computed to assess the performance of each band with field-measured values. Spectral data of 25 sample plots were collected from ASD spectrometer by using 0.25 m × 0.25 m square frame to compare the performance.

Results

Calibration target

In this study, five calibration panels and one pseudo target were used to collect the field spectra for the quantification of image DN to surface reflectance. Figure 3 shows the spectral reflectance of each calibration panel. The mean reflectance value of each target for each spectral region of sensor waveband was plotted. The results show an increase in reflectance associated with the decrease in grey level. Results of this study showed that white pseudo target represents maximum reflectance whereas, minimum reflectance is covered by dark antracit calibration panel. These two panels covered both the extremes of reflectance and can be used to prepare the predication equation for each image. Remaining four panels covered the middle portion of spectral reflectance ranging from ~10% to ~60%.

The reflectance value of white target was gradually decreasing from 570 to 800 nm wavelength. However, the reflectance of calibration panel remained the same from 570 to 800 nm wavelengths. In contrast, there was a sharp increase in reflectance of cream panel from 530 to 570 nm and a slight increase in pearl target from 530 to 570 nm.

Predication equation

The combination of calibration panels and field targets enabled the development of linear relationship between image DN and surface reflectance. Six targets (five calibration and one pseudo calibration) were used to derive the calibration equation from all images. Figure 4 shows the linear fit and coefficient of determination between image DN and spectral reflectance measured in the field from each calibration target. Results showed statistically significant relationship in all spectral bands. Coefficient of determination R^2 = 0.97–0.99 was achieved in all bands, indicating that relationship between the image DN and reflectance is linear. At the wavelengths of 530, 550, 570, 700 and 800 nm, equation showed R^2 = 0.99 and at 670 nm, the equation showed R^2 = 0.97 (Figure 4(a, d)). The use of pseudo target showed maximum reflectance in all equations ranging from ~0.75% to ~0.85%. This white colour plastic target ensures that predicated reflectance values were interpreted within the limits of the predication equation. While, dark antracit calibration panel reflectance values covered the lower end of predication equation ranging from 0.059% to 0.062%. Predication equation of all images showed that the value of y-intercept was very small and was compatible to zero and thus, can be excluded from calculation (Table 2).

Simplified predication equation

Based on six calibration targets, it was found that the relationship between image raw DN and the spectral reflectance values is linear and y-intercept of the predication equation can be used as a constant parameter for each waveband, which is in accordance with the results of Del Pozo et al. (2014). By considering

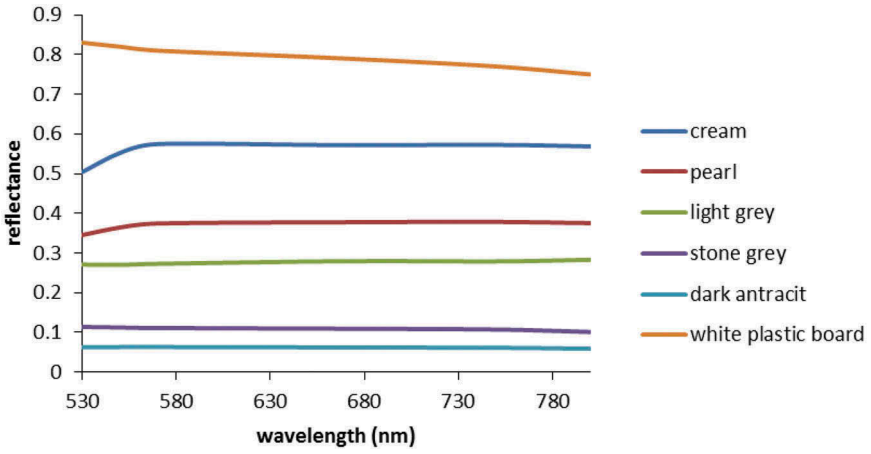

Figure 3. Mean spectral signature from 530 to 800 nm of the calibration panels obtained in the field using ASD spectroradiometer.

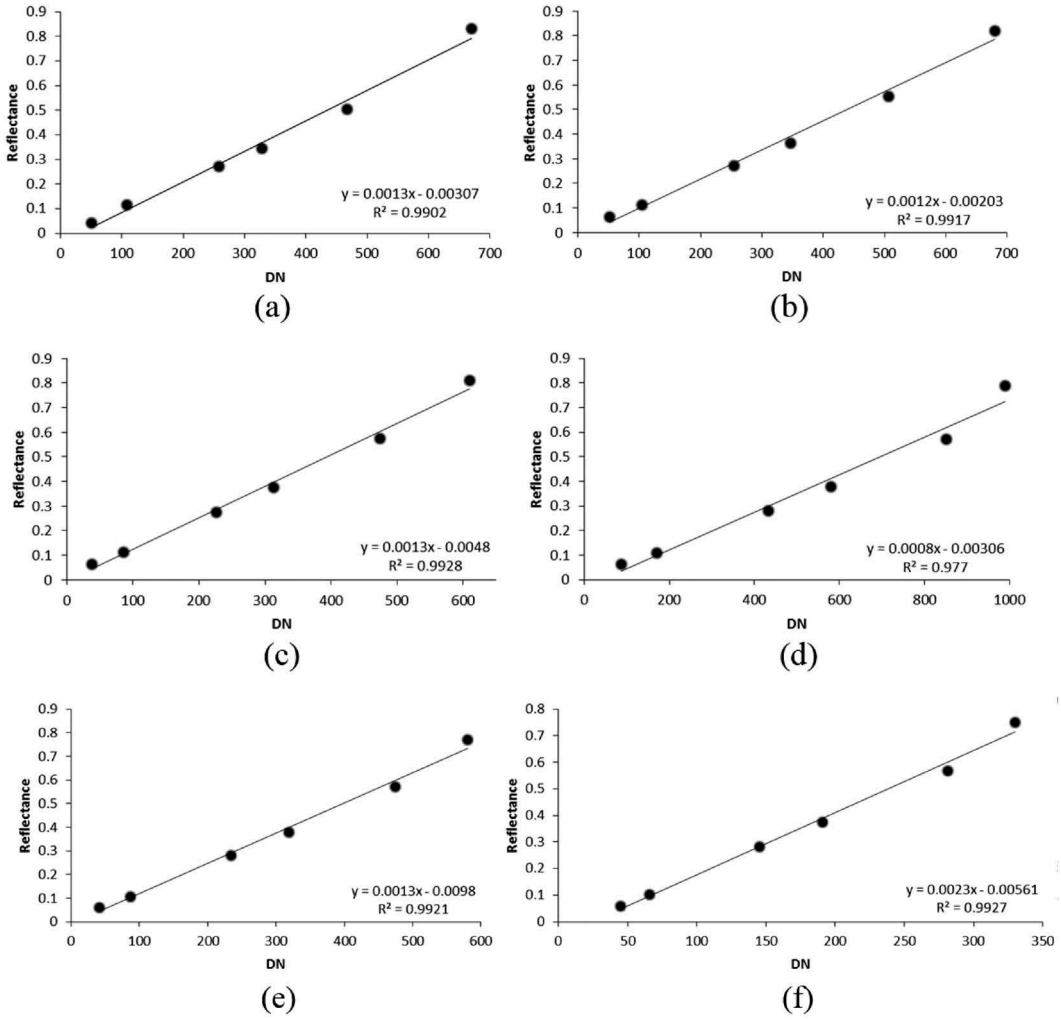

Figure 4. Relationship between mean image DN and mean reflectance of the calibration panels for each waveband of Mini-MCA sensor. Each data point represents one calibration target. (a) 530 nm, (b) 550 nm, (c) 570, (d) 670 nm, (e) 700 nm and (f) 800 nm.

Table 2. Mini-MCA calibration constant (*y*-intercept).

Wavelength	530	550	570	670	750	800
Y-intercept	−0.00307	−0.00203	−0.0048	−0.00306	−0.0098	−0.00561

reflectance of dark target as zero (starting point of equation as zero), only one target was required to cover the brightest portion of image. This process made the conversion of DN to reflectance easy to adopt. Table 3 shows the calibration equation for each single waveband with summary statistics derived from validation targets. The overall RMSE value of each band showed that there was high degree of agreement between the UAS-driven reflectance and field-measured reflectance for calibration targets.

Table 3. Summary statistics derived from the simplified predication calibration equation for each waveband of Mini-MCA.

Channel	Simplified predication equation	RMSE (%)	MAPE%
530	$\rho_y = 0.0013 \times \mathrm{DN}$	0.063	16.56
550	$\rho_y = 0.0012 \times \mathrm{DN}$	0.060	15.56
570	$\rho_y = 0.0013 \times \mathrm{DN}$	0.025	7.82
670	$\rho_y = 0.0008 \times \mathrm{DN}$	0.064	17.16
750	$\rho_y = 0.0013 \times \mathrm{DN}$	0.027	7.72
800	$\rho_y = 0.0023 \times \mathrm{DN}$	0.054	29.11

Two out of five bands recorded RMSE values below 0.025%, while 570 nm band recoded the lowest RMSE value 0.025%. The Mean Absolute Percent Error (MAPE) values of 570 and 750 nm bands were also in agreement with the RMSE values of 570 and 750 nm bands and showed lowest values of 7.72 and 7.82. The 530, 670 and 550 nm bands recorded the highest RMSE values of 0.063%, 0.064% and 0.060%, respectively. The RMSE value of 800 nm band was 0.054%. However, the MAPE value showed that the 800 nm bands recorded highest error in the spectrum.

Surface reflectance comparison

Radiometrically calibrated image-driven surface reflectance was compared to field-measured reflectance using ASD. The green crop cover showed sharp rise in the

surface reflectance values from 700 to 800 nm. The comparison of image-driven surface reflectance and field-measured surface reflectance of green crop is illustrated in Figure 5(a). The prediction outcomes showed that the image-driven results were predicting less reflectance as compared to the ASD reflectance results in all bands. For the 530 and 550 nm bands, the surface reflectance values reduced to 0.0114% in relation to the ASD measurements. In case of 670 and 700 nm bands, reflectance reduction was 0.0157% and 0.0063% respectively. Highest underestimation of 0.057% was observed in case of 800 nm band and the least underestimation was observed in 570 nm band with an average reduction of 0.0043%.

The results obtained for diseased and dry vegetation are illustrated in Figure 5(b). For the 530 and 550 nm bands, the surface reflectance values reduced to 0.0025% and 0.0023% respectively in relation to the ASD measurement. In case of 670 and 700 nm bands, reflectance reduction was 0.0022% and 0.0030%, respectively. Highest underestimation of 0.0110% was observed in case of 800 nm band and the least underestimation was observed in 570 nm band with an average reduction of 0.0019%.

The compression of dry soil reflectance from image and ASD is presented in Figure 5©. For the 530 and 550 nm band, the surface reflectance values diminished to 0.0048% and 0.0032%, respectively. Highest underestimation of 0.0169% was observed in case of 800 nm band and the least underestimation was observed in 570 nm band with an average reduction of 0.0023%. In case of 670 and 700 nm bands, reflectance reduction was 0.0062% and 0.0051%, respectively. In case of moist soil, the highest underestimation of 0.0071% was observed in case of 800 nm band and the least underestimation was observed in 700 nm band with an average reduction of 0.0006% (Figure 5(d)). For the 530 and 570 nm bands, the surface reflectance values were underestimated to 0.0019% and 0.0021%, respectively. The reflectance values of 550 and 670 nm bands were reduced to 0.0025%.

Discussion

Real time, fast and accurate processing of UAS imagery is an area of active research and is the future of RS technologies. In this research, the analysis was carried out to perform radiometric calibration of UAS images. Generally, empirical line method with multiple calibration targets is used to convert raw image DN to surface reflectance, which requires cost intensive calibration panels with lambertian properties (Del Pozo et al., 2014; Herrero-Huerta et al., 2014; Miura & Huete, 2009; Teillet, Fedosejevs, Thome, & Barker, 2007). In this study, the empirical line method for radiometric calibration used was unlike the methods used in previous literature (Del Pozo et al., 2014; Herrero-Huerta et al., 2014; Miura & Huete, 2009; Teillet et al., 2007).

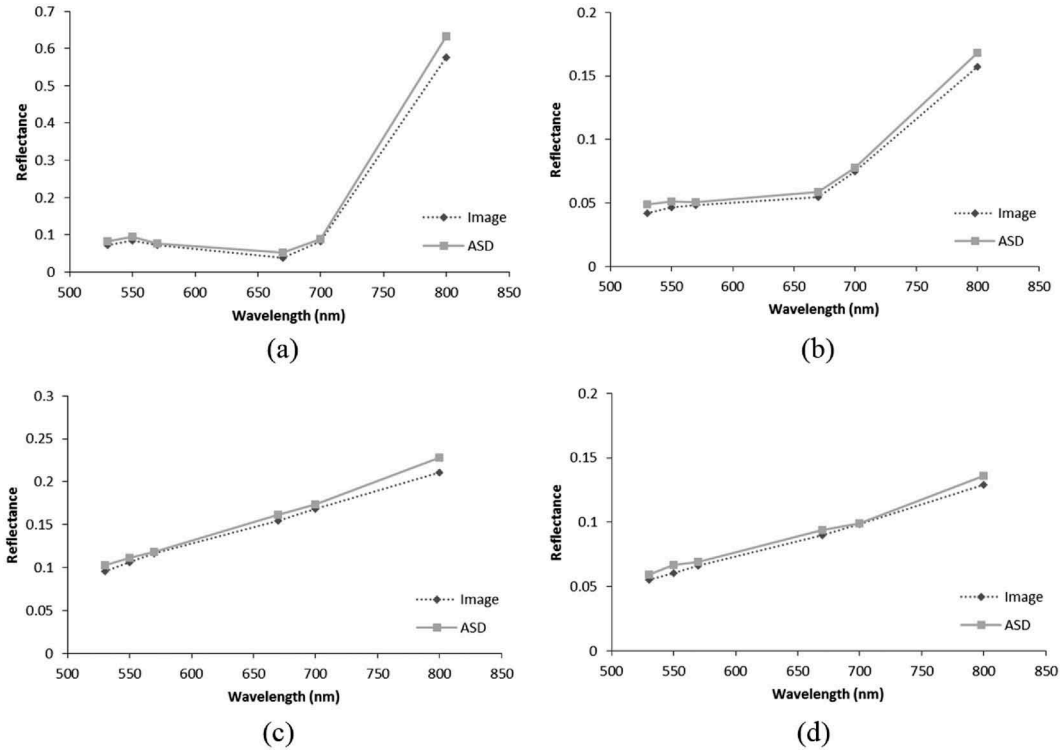

Figure 5. Reflectance estimated from ground measurement and UAS data (530, 550, 570, 670, 750 and 800 nm). Each data point represents reflectance values of poppy crop (a), diseased plants (b), dry soil (c) and wet soil (d).

In case of satellite imagery, satellites are equipped with advanced systems that collect the information on weather and sun illumination conditions and record the metadata corresponding to each image as a header file. Metadata provides the calibration coefficients which help researchers to rectify the data before further processing. Moreover, a large amount of investigation has already been done on satellite data that makes calibration process more standardised, whereas, no standardised process is available for UAS RS. UAS-mounted sensor provides cost effective solution to collect the RS data at required time. Although, widely used UAS sensors do not collect illumination-specific data, yet advanced UAS sensors are coming with sunshine sensors that are capable of collecting illumination condition data and thus, allows to calibrate the data. In this research, the sensor used did not contain data on illumination conditions, thus, the intensity of the ambient light would have varied due to the sky being overcast for some time. Therefore, the amount of reflected light energy from the surface must have altered resulting in error in data accuracy. To cope with illumination variability, accurate calibration is imperative. Studies that have carried out calibration for elimination of errors due to changes in weather and illumination for UAS-mounted sensors may not be replicated to other regions due to differences in site conditions. As a standardised method for radiometric calibration of UAS-based imagery does not exist, therefore, this study tested an empirical line method using only one pseudo calibration target per image to make the process simpler and replicable without compromising on accuracy. This method uses only one pseudo calibration target per image to build empirical line calibration equations, instead of two or more lambertian calibration targets, which has dramatically simplified the procedure to conduct field campaign. In this study, the results demonstrated the feasibility and usefulness of using pseudo calibration targets (white plastic board) as compared to calibration targets with lambertian properties that are expensive, thus reducing the cost of UAS campaign. This method requires one pseudo target in each image, thus, allowing each image to be rectified with the help of that target resulting in a homogeneous image mosaic.

For the development of an empirical line equation, at least two data points are required. The results achieved showed that the first point for the equation can be considered as zero representing the minimum reflectance detected by the sensor, whereas, the second point can be taken as the reading of one pseudo target. In such case, the slope and DN value of the image can be used to convert DN values to surface reflectance making the process more robust and replicable.

The pseudo target used in this study was found to be highly lambertian, although, it did not provide equal reflectance at different wavelengths (Figure 3). Relatively more reflectance was observed in the visible region than the Near Infrared (NIR) region of the spectrum and gradual decrease in reflectance was observed from 530 to 800 nm. Therefore, one calibration equation was required for each band image (n = 6). It was assumed that the reflectance of pseudo calibration target does not change abruptly. Moreover, the protocol used to collect the ASD field measurement also allowed to mitigate the changes in reflectance over the time and to minimise the effect of changing illumination condition, whereas, UAS image recorded DNs of a target do change with changing illumination condition. As a result, UAS image acquired in clear and sunny condition could show high DN values and lower DNs in cloudy condition. Similarly, the change in sun angle due to changing seasons also influences the DN values of the image (Wang & Myint, 2015). Thus, change in illumination condition alters the slope and offset of empirical line equation, and if implemented elsewhere, would require a new empirical line equation based on field-measured reflectance data.

The result of our study demonstrated that the y-intercept value is near zero and do not change over time and can be taken as the minimum amount of reflected light that can be recorded by each CMOS image sensor (n = 6). This is an inherent property of the sensor and does not change abruptly, whereas, it can be changed over longer time associated to sensor stability (Del Pozo et al., 2014; Herrero-Huerta et al., 2014). Therefore, for each empirical line equation y-intercept can be considered as zero as a first data point and value of pseudo calibration target can be used as a second point to develop empirical line equation (Table 3). This allows the derivation of surface reflectance with the RMSE ranging from 0.025% to 0.064% (Table 3). Highest MPAE of 29.11% was observed in 800 nm band and least MPAE of 7.82% was observed in 570 nm band. Results obtained from single pseudo target calibration method proves that it can be used as radiometric calibration target, which is in accordance with the results obtained with digital camera (Wang & Myint, 2015).

The comparison of calibrated image-driven surface reflectance to field-measured reflectance showed that each band is underestimating the reflectance in all bands ranging from 0.0169% to 0.0006%. Highest difference was observed in 800 nm band and least was observed in case of 700 nm band. Relatively less accuracy can be associated to the material used for calibration panel; as white plastic board reflects more light, although, spectral reflectance alters by changing surface roughness and thinness of board (Ham, Kluitenberg, & Lamont, 1993; Hoppert & LaPlante, 1992; Moroni, Mei, Leonardi, Lupo, & La, 2015).

Plastic board made with polyethylene terephthalate, polycarbonate and polymethyl methacrylate provide almost consistent spectral signatures in visible portion, whereas. Signatures slightly decline at near-infrared region (Moroni et al., 2015). Moreover, it is associated to sensors sensitivity at far end range at 800 nm where more light passes through filter. The highest error is observed in case of vegetation 0.057% and it is reduced in case of moist soil to 0.0071%. Relatively highest error in case of vegetation reflectance is associated to angular reflectance, crop heterogeneity and difference of scale (Baugh & Groeneveld, 2008; Herrero-Huerta et al., 2014). Overall the difference of reflectance is very small and can be ignored, thus, it can considered as a step forward for UAS image calibration in accordance with the findings of previous studies (Del Pozo et al., 2014; Herrero-Huerta et al., 2014; Staben et al., 2012; Wang & Myint, 2015). Although, proposed method can provide easy and cost effective calibration method and has dramatically simplified the procedure and reduced the field workload, there exist some limitations when implementing for other sensors. Calibration parameters vary for every sensor, and the sensitivity of sensors differ from each other. Thus, the lowest possible reflectance of zero observed with this sensor, may not be measured with other sensors. Therefore, to check the applicability of this method on other sensors, calibration equations for each sensor bands need to be developed using multiple targets and tested with the proposed method before implementation. It is recommended to use white pseudo target as it will cover the maximum possible reflectance. Moreover, the size of a calibration target should be large enough to cover large number of pixel in each target (Smith & Milton, 1999). Overall, proposed methodology is very useful for precision agriculture applications and can assist to calibrate UAS images using single calibration target.

Conclusion

This paper describes a successful methodology for radiometric calibration using low-cost single pseudo target method for each image of a Mini-MCA sensor. The quantitative analysis of field measured and image estimated reflectance confirms the validity of the proposed method. For this purpose, UAS two flight campaigns were conducted over a study area with distributed pseudo and calibration targets for converting DN values to spectral reflectance. Calibration equation derived from radiometric calibration targets was simplified by using two points, first point (y-intercept) zero and second point was used as the DN and reflectance of white pseudo target. The result achieved from this method provided accurate and cost effective solution for radiometric calibration of UAS-based images. Based on the results from this study, it can be concluded that a single pseudo target-based calibration method can be used for easy and accurate UAS-based image calibration.

Acknowledgements

Author would like to acknowledge Arko Lucieer and Darren Turner for organising and conducting the UAS field campaign. Also, special thanks are conveyed to Iain Clarke for his help in conducting the GPS survey for this research project. Special thanks are conveyed to Zbynek Malenovsk for his help during UAV and spectral campaign. This research work was supported and funded by the University of Tasmania, Australia.

Disclosure statement

No potential conflict of interest was reported by the author.

Funding

This research work was supported and funded by the University of Tasmania, Australia.

ORCID

Faheem Iqbal http://orcid.org/0000-0003-3034-5707

References

Ajayan, P.M., & Tour, J.M. (2007). Materials science: Nanotube composites. *Nature*, *447*(7148), 1066–1068. doi:10.1038/4471066a

Bakhsh, A., & Kanwar, R., 2006. GIS and cluster analysis of NO3-N leaching losses to subsurface drainage water. *2006 International Conference on Advances in Space Technologies*.

Baluja, J., Diago, M.P., Balda, P., Zorer, R., Meggio, F., Morales, F., & Tardaguila, J. (2012). Assessment of vineyard water status variability by thermal and multispectral imagery using an unmanned aerial vehicle (UAV). *Irrigation Science*, *30*(6), 511–522. doi:10.1007/s00271-012-0382-9

Bastiaanssen, W.G., Molden, D.J., & Makin, I.W. (2000). Remote sensing for irrigated agriculture: Examples from research and possible applications. *Agricultural Water Management*, *46*(2), 137–155. doi:10.1016/S0378-3774(00)00080-9

Bastiaanssen, W.G.M., & Ali, S. (2003). A new crop yield forecasting model based on satellite measurements applied across the Indus Basin, Pakistan. *Agriculture, Ecosystems & Environment*, *94*(3), 321–340. doi:10.1016/S0167-8809(02)00034-8

Baugh, W.M., & Groeneveld, D.P. (2008). Empirical proof of the empirical line. *International Journal of Remote Sensing*, *29*(3), 665–672. doi:10.1080/01431160701352162

Bendig, J., Bolten, A., & Bareth, G. (2013). UAV-based imaging for multi-temporal, very high resolution crop surface models to monitor crop growth variability. *Photogrammetrie - Fernerkundung - Geoinformation*, *2013*(6), 551–562. doi:10.1127/1432-8364/2013/0200

Bendig, J., Bolten, A., Bennertz, S., Broscheit, J., Eichfuss, S., & Bareth, G. (2014). Estimating biomass of barley using crop surface models (CSMs) derived from UAV-based RGB imaging. *Remote Sensing*, *6*(11), 10395–10412. doi:10.3390/rs61110395

Berni, J.A., Zarco-Tejada, P.J., Suarez, L., & Fereres, E. (2009a). Thermal and narrowband multispectral remote sensing for vegetation monitoring from an unmanned aerial vehicle. *IEEE Transactions on Geoscience and Remote Sensing*, *47*(3), 722–738. doi:10.1109/TGRS.2008.2010457

Berni, J.A.J., Zarco-Tejada, P.J., Sepulcre-Canto, G., Fereres, E., & Villalobos, F. (2009). Mapping canopy conductance and CWSI in olive orchards using high resolution thermal remote sensing imagery. *Remote Sensing of Environment*, *113*(11), 2380–2388. doi:10.1016/j.rse.2009.06.018

Berni, J.A.J., Zarco-Tejada, P.J., Suarez, L., & Fereres, E. (2009b). Thermal and narrowband multispectral remote sensing for vegetation monitoring from an unmanned aerial vehicle. *IEEE Transactions on Geoscience and Remote Sensing*, *47*(3), 722–738. doi:10.1109/TGRS.2008.2010457

Boschetti, L., Flasse, S.P., & Brivio, P.A. (2004). Analysis of the conflict between omission and commission in low spatial resolution dichotomic thematic products: The pareto boundary. *Remote Sensing of Environment*, *91*(3), 280–292. doi:10.1016/j.rse.2004.02.015

Brandao, Z.N., Sofiatti, V., Bezerra, J.R.C., Ferreira, G.B., & Medeiros, J.C. (2015). Spectral reflectance for growth and yield assessment of irrigated cotton. *Australain Journal of Crop Science*, *9*(1), 75–84.

Carbone, G.J., Narumalani, S., & King, M. (1996). Application of remote sensing and GIS technologies with physiological crop models. *Photogrammetric Engineering and Remote Sensing*, *62*(2), 171–179.

Chavez, P.S., Jr. (1989). Radiometric calibration of landsat thematic mapper multispectral images. *Photogrammetric Engineering and Remote Sensing*, *55*(9), 1285–1294.

Cheng, Y.B., Zarco-Tejada, P.J., Riano, D., Rueda, C.A., & Ustin, S.L. (2006). Estimating vegetation water content with hyperspectral data for different canopy scenarios: Relationships between AVIRIS and MODIS indexes. *Remote Sensing of Environment*, *105*(4), 354–366. doi:10.1016/j.rse.2006.07.005

Cohen, Y., Alchanatis, V., Meron, M., Saranga, Y., & Tsipris, J. (2005). Estimation of leaf water potential by thermal imagery and spatial analysis. *Journal of Experimental Botany*, *56*(417), 1843–1852. doi:10.1093/jxb/eri174

Del Pozo, S., Rodríguez-Gonzálvez, P., Hernández-López, D., & Felipe-García, B. (2014). Vicarious radiometric calibration of a multispectral camera on board an unmanned aerial system. *Remote Sensing*, *6*(3), 1918–1937. doi:10.3390/rs6031918

Dempewolf, J., Adusei, B., Becker-Reshef, I., Hansen, M., Potapov, P., Khan, A., & Barker, B. (2014). Wheat yield forecasting for Punjab province from vegetation index time series and historic crop statistics. *Remote Sensing*, *6*(10), 9653–9675. doi:10.3390/rs6109653

Fedotov, Y., & Osmani, Z.A. (2010). *Afghanistan Opium Survey 2010*. United Nations officer on drugs and Crime, Minstry of Counter Narcotics, Kabul.

French, A.N., Hunsaker, D.J., & Thorp, K.R. (2015). Remote sensing of environment remote sensing of evapotranspiration over cotton using the TSEB and METRIC energy balance models □. *Remote Sensing of Environment*, *158*, 281–294. doi:10.1016/j.rse.2014.11.003

Geipel, J., Link, J., & Claupein, W. (2014). Combined spectral and spatial modeling of corn yield based on aerial images and crop surface models acquired with an unmanned aircraft system. *Remote Sensing*, *6*(11), 10335–10355. doi:10.3390/rs61110335

Ham, J.M., Kluitenberg, G.J., & Lamont, W.J. (1993). Optical properties of plastic mulches affect the field temperature regime. *Journal of the American Society for Horticultural Science*, *118*(2), 188–193.

Harwin, S., & Lucieer, A. (2012). Assessing the accuracy of georeferenced point clouds produced via multi-view stereopsis from unmanned aerial vehicle (UAV) imagery. *Remote Sensing*, *4*(12), 1573–1599. doi:10.3390/rs4061573

Herrero-Huerta, M., Hernández-López, D., Rodriguez-Gonzalvez, P., González-Aguilera, D., & González-Piqueras, J. (2014). Vicarious radiometric calibration of a multispectral sensor from an aerial trike applied to precision agriculture. *Computers and Electronics in Agriculture*, *108*, 28–38. doi:10.1016/j.compag.2014.07.001

Hoppert, B.D., & LaPlante, D.J. (1992). *Enhanced metal filter/mirror coatings for use on engineering plastics. Google Patents. US patent 5, 169,229.*

Iqbal, F. (2011). Detection of salt affected soil in rice-wheat area using satellite image. *African Journal of Agriculture Research*, *6*(21), 4973–4982.

Jaakkola, A., Hyyppa, J., Kukko, A., Yu, X.W., Kaartinen, H., Lehtomaki, M., & Lin, Y. (2010). A low-cost multi-sensoral mobile mapping system and its feasibility for tree measurements. *ISPRS Journal of Photogrammetry and Remote Sensing*, *65*(6), 514–522. doi:10.1016/j.isprsjprs.2010.08.002

Joseph, W., Aerts, S., Vandenbossche, M., Thielens, A., & Martens, L. (2016). Drone based measurement system for radiofrequency exposure assessment. *Bioelectromagnetics*, *37*(3), 195–199. doi:10.1002/bem.v37.3

Karpouzli, E., & Malthus, T. (2003). The empirical line method for the atmospheric correction of IKONOS imagery. *International Journal of Remote Sensing*, *24*(5), 1143–1150. doi:10.1080/0143116021000026779

Kaur, R., Singh, B., Singh, M., & Thind, S.K. (2015). Hyperspectral indices, correlation and regression models for estimating growth parameters of wheat genotypes. *Journal of the Indian Society of Remote Sensing*. doi:10.1007/s12524-014-0425-1

Kelcey, J., & Lucieer, A. (2012). Sensor correction of a 6-band multispectral imaging sensor for UAV remote sensing. *Remote Sensing*, *4*(5), 1462–1493.

Kross, A., McNairn, H., Lapen, D., Sunohara, M., & Champagne, C. (2015). Assessment of RapidEye vegetation indices for estimation of leaf area index and biomass in corn and soybean crops. *International Journal of Applied Earth Observation and Geoinformation*, *34*, 235–248. doi:10.1016/j.jag.2014.08.002

Larson, W.E., & Robert, P.C. (1991). Farming by soil. In *Soil management for sustainability*, Soil Water Conserv. Soc., Ankeny, IA (pp. 103–112).

Lausch, A., Pause, M., Merbach, I., Zacharias, S., Doktor, D., Volk, M., & Seppelt, R. (2013). A new multiscale approach for monitoring vegetation using remote sensing-based indicators in laboratory, field, and landscape. *Environmental Monitoring and Assessment*, *185*(2), 1215–1235. doi:10.1007/s10661-012-2627-8

Leroux, L., Jolivot, A., Bégué, A., Lo, S.D., & Zoungrana, B. (2014). How reliable is the MODIS land cover product for crop mapping sub-Saharan agricultural landscapes? *Remote Sensing*, *6*(9), 8541–8564. doi:10.3390/rs6098541

Lucieer, A., De Jong, S., & Turner, D. (2013). Mapping landslide displacements using structure from motion (SfM) and image correlation of multi-temporal UAV photography. *Progress in Physical Geography*, *38*(1) 97–116.

Lucieer, A., Malenovský, Z., Veness, T., & Wallace, L. (2014). HyperUAS-imaging spectroscopy from a multi-rotor unmanned aircraft system. *Journal of Field Robotics*, *31*(4), 571–590. doi:10.1002/rob.2014.31.issue-4

Mäkynen, J., Saari, H., Holmlund, C., Mannila, R., & Antila, T. (2012). *Multi- and hyperspectral UAV imaging system for forest and agriculture applications*International Society for optices and photonics, USA.

Mattar, C., Hernández, J., Santamar'ia-Artigas, A., Durán-Alarcón, C., Olivera-Guerra, L., Inzunza, M., … Escobar-Lav'in, E. (2014). A first in-flight absolute calibration of the Chilean Earth Observation Satellite. *ISPRS Journal of Photogrammetry and Remote Sensing*, *92*, 16–25. doi:10.1016/j.isprsjprs.2014.02.017

Miura, T., & Huete, A.R. (2009). Performance of three reflectance calibration methods for airborne hyperspectral spectrometer data. *Sensors (Basel, Switzerland)*, *9*(2), 794–813. doi:10.3390/s90200794

Moran, M.S., Bryant, R., Thome, K., Ni, W., Nouvellon, Y., Gonzalez-Dugo, M.P., … Clarke, T.R. (2001). A refined empirical line approach for reflectance factor retrieval from Landsat-5 TM and Landsat-7 ETM+. *Remote Sensing of Environment*, *78*(1), 71–82. doi:10.1016/S0034-4257(01)00250-4

Morel, J., Todoroff, P., Bégué, A., Bury, A., Martiné, J.-F., & Petit, M. (2014). Toward a satellite-based system of sugarcane yield estimation and forecasting in smallholder farming conditions: A case study on reunion Island. *Remote Sensing*, *6*(7), 6620–6635. doi:10.3390/rs6076620

Moroni, M., Mei, A., Leonardi, A., Lupo, E., & La, M.F. (2015). PET and PVC separation with hyperspectral imagery. *Sensors*, *15*(1), 2205–2227. doi:10.3390/s150102205

Mulla, D.J. (2013). Twenty five years of remote sensing in precision agriculture: Key advances and remaining knowledge gaps. *Biosystems Engineering*, *114*(4), 358–371. doi:10.1016/j.biosystemseng.2012.08.009

Oøvergaard, S.I., Isaksson, T., Kvaalc, K., & Korsaeth, A. (2010). Comparisons of two hand-held, multispectral field radiometers and a hyperspectral airborne imager in terms of predicting spring wheat grain yield and quality by means of powered partial least squares regression. *Journal of near Infrared Spectroscopy*, *18*(4), 247–261. doi:10.1255/jnirs.892

Oudemans, P.V., Pozdnyakova, L., Hughes, M.G., & Rahman, F. (2002). GIS and remote sensing for detecting yield loss in cranberry culture. *Journal of Nematology*, *34*(3), 207–212.

Papadavid, G., Hadjimitsis, D., Toulios, L., & Michaelides, S. (2011). Mapping potato crop height and leaf area index through vegetation indices using remote sensing in Cyprus. *Journal of Applied Remote Sensing*, *5*(1), 53526. doi:10.1117/1.3596388

Pinter, P.J., Jr, Hatfield, J.L., Schepers, J.S., Barnes, E.M., Moran, M.S., Daughtry, C.S.T., & Upchurch, D.R. (2003). Remote sensing for crop management. *Photogrammetric Engineering & Remote Sensing*, *69*(6), 647–664. doi:10.14358/PERS.69.6.647

Rango, A., Laliberte, A., Herrick, J.E., Winters, C., Havstad, K., Steele, C., & Browning, D.; others. (2009). Unmanned aerial vehicle-based remote sensing for rangeland assessment, monitoring, and management. *Journal of Applied Remote Sensing*, *3*(1), 33542. doi:10.1117/1.3216822

Saari, H., Pellikka, I., Pesonen, L., Tuominen, S., Heikkilä, J., Holmlund, C., … Antila, T. (2011). *Unmanned aerial vehicle (UAV) operated spectral camera system for forest and agriculture applications*.Proceedings of the SPIE, Remote Sensing for Agriculture, Ecosystems, and Hydrology XIII, Prague, Czech Republic.

Smith, G.M., & Milton, E.J. (1999). The use of the empirical line method to calibrate remotely sensed data to reflectance. *International Journal of Remote Sensing*, *20*(13), 2653–2662. doi:10.1080/014311699211994

Staben, G.W., Pfitzner, K., Bartolo, R., & Lucieer, A. (2012). Empirical line calibration of WorldView-2 satellite imagery to reflectance data: Using quadratic prediction equations. *Remote Sensing Letters*, *3*(6), 521–530. doi:10.1080/01431161.2011.609187

Stadler, A., Rudolph, S., Kupisch, M., Langensiepen, M., van der Kruk, J., & Ewert, F. (2015). Quantifying the effects of soil variability on crop growth using apparent soil electrical conductivity measurements. *European Journal of Agronomy*, *64*, 8–20. doi:10.1016/j.eja.2014.12.004

Stafford, J.V. (2000). Implementing precision agriculture in the 21st century. *Journal of Agricultural Engineering Research*, *76*(3), 267–275. doi:10.1006/jaer.2000.0577

Stagakis, S., González-Dugo, V., Cid, P., Guillén-Climent, M.L., & Zarco-Tejada, P.J. (2012). Monitoring water stress and fruit quality in an orange orchard under regulated deficit irrigation using narrow-band structural and physiological remote sensing indices. *ISPRS Journal of Photogrammetry and Remote Sensing*, *71*, 47–61. doi:10.1016/j.isprsjprs.2012.05.003

Stellman, C.M., Olchowski, F.M., & Michalowicz, J.V. (2001). *WAR HORSE(wide area reconnaissance – hyperspectral overhead real-time surveillance experiment)*. Proceeding SPIE, (4379) 339–346.

Stevens, A., & Ramirez-Lopez, L., 2014. An introduction to the prospectr package. *R Package Vignette, Report No.: R Package Version 0.1*, 3.

Stow, D., Hope, A., Nguyen, A.T., Phinn, S., & Benkelman, C.A. (1996). Monitoring detailed land surface changes using an airborne multispectral digital camera system. *IEEE Transactions on Geoscience and Remote Sensing*, *34*(5), 1191–1203. doi:10.1109/36.536536

Swain, K.C., Thomson, S.J., & Jayasuriya, H.P.W. others. (2010). Adoption of an unmanned helicopter for low-altitude remote sensing to estimate yield and total biomass of a rice crop. *Transactions of the ASAE (American Society of Agricultural Engineers)*, *53*(1), 21.

Teillet, P.M., Fedosejevs, G., Thome, K.J., & Barker, J.L. (2007). Impacts of spectral band difference effects on radiometric cross-calibration between satellite sensors in the solar-reflective spectral domain. *Remote Sensing of Environment*, *110*(3), 393–409. doi:10.1016/j.rse.2007.03.003

Thornton, P. (2002). *Mapping poverty and livestock in the developing world*. ILRI, Kenya (aka ILCA and ILRAD).

Torres-Sánchez, J., López-Granados, F., & Peña, J.M. (2015). An automatic object-based method for optimal thresholding in UAV images: application for vegetation detection in herbaceous crops. *Computers and Electronics in Agriculture*, *114*, 43–52. doi:10.1016/j.compag.2015.03.019

Turner, D., Lucieer, A., & Watson, C. (2012). An automated technique for generating georectified mosaics from ultra-high resolution unmanned aerial vehicle (UAV) imagery, based on structure from motion (SfM) point clouds. *Remote Sensing*, *4*(5), 1392–1410. doi:10.3390/rs4051392

Uto, K., Seki, H., Saito, G., & Kosugi, Y. (2013). Characterization of rice paddies by a UAV-mounted miniature hyperspectral sensor system. *IEEE Journal of Selected Topics in Applied Earth Observations and Remote Sensing*. doi:10.1109/JSTARS.2013.2250921

Vicente-Serrano, S.M., Pérez-Cabello, F., & Lasanta, T. (2008). Assessment of radiometric correction techniques in analyzing vegetation variability and change using time series of Landsat images. *Remote Sensing of Environment*, *112*(10), 3916–3934. doi:10.1016/j.rse.2008.06.011

Waine, T.W., Simms, D.M., Taylor, J.C., & Juniper, G.R. (2014). Towards improving the accuracy of opium yield estimates with remote sensing. *International Journal of Remote Sensing*, *35*(16), 6292–6309. doi:10.1080/01431161.2014.951743

Wang, C., & Myint, S.W. (2015). A simplified empirical line method of radiometric calibration for small unmanned aircraft systems-based remote sensing. *IEEE Journal of Selected Topics in Applied Earth Observations and Remote Sensing*, *8*(5), 1876–1885. doi:10.1109/JSTARS.2015.2422716

Warren, C.P., Pfister, W., Even, D., Velasco, A., Yee, S., Breitwieser, D., & Naungayan, J. (2011). *Miniaturization of a SWIR hyperspectral imager*.

Whiting, M.L., Ustin, S.L., Zarco-Tejada, P., Palacios-Orueta, A., Vanderbilt, V.C., & Spie (2006). Hyperspectral mapping of crop and soils for precision agriculture. In: *Conference on Remote Sensing and Modeling of Ecosystems for Sustainability III*. San Diego, CA: Spie-Int Soc Optical Engineering.

Zarco-Tejada, P.J., Guillen-Climent, M.L., Hernandez-Clemente, R., Catalina, A., Gonzalez, M.R., & Martin, P. (2013). Estimating leaf carotenoid content in vineyards using high resolution hyperspectral imagery acquired from an unmanned aerial vehicle (UAV). *Agricultural and Forest Meteorology*, *171*, 281–294. doi:10.1016/j.agrformet.2012.12.013

Zarco-Tejada, P.J., Miller, J.R., Morales, A., Berjon, A., & Aguera, J. (2004). Hyperspectral indices and model simulation for chlorophyll estimation in open-canopy tree crops. *Remote Sensing of Environment*, *90*(4), 463–476. doi:10.1016/j.rse.2004.01.017

Zarco-Tejada, P.J., Ustin, S.L., & Whiting, M.L. (2005a). Temporal and spatial relationships between within-field yield variability in cotton and high-spatial hyperspectral remote sensing imagery. *Agronomy Journal*, *97*(3), 641–653. doi:10.2134/agronj2003.0257

Zarco-Tejada, P.J., Ustin, S.L., & Whiting, M.L. (2005b). Temporal and spatial relationships between within-field yield variability in cotton and high-spatial hyperspectral remote sensing imagery. *Agronomy Journal*, *97*(3), 641–653. doi:10.2134/agronj2003.0257

Zhang, C.H., & Kovacs, J.M. (2012). The application of small unmanned aerial systems for precision agriculture: A review. *Precision Agriculture*, *13*(6), 693–712. doi:10.1007/s11119-012-9274-5

Zhang, N., Wang, M., & Wang, N. (2002). Precision agriculture a worldwide overview. *Computers and Electronics in Agriculture*, *36*(2), 113–132. doi:10.1016/S0168-1699(02)00096-0

Zhou, X., Zheng, H.B., Xu, X.Q., He, J.Y., Ge, X.K., Yao, X., … Tian, Y.C. (2017). Predicting grain yield in rice using multi-temporal vegetation indices from UAV-based multispectral and digital imagery. *ISPRS Journal of Photogrammetry and Remote Sensing*, *130*, 246–255. doi:10.1016/j.isprsjprs.2017.05.003

Zhu, J., Wang, K., Deng, J., & Harmon, T. (2010). *Quantifying nitrogen status of rice using low altitude UAV-mounted system and object-oriented segmentation methodology*. 603–609.ASME 2009 International Design Engineering Technical Conferences and Computers and Information in Engineering Conference, American Society of Mechanical Engineers.

Zhu, Y.T., Lowe, T.C., & Langdon, T.G. (2004). Performance and applications of nanostructured materials produced by severe plastic deformation. *Scripta Materialia*, *51*(8), 825–830. doi:10.1016/j.scriptamat.2004.05.006